Quantum oscillations and Fermi surfaces of Sn- and Pb-doped Bi

1994 J. Phys.: Condens. Matter 6 3707

(http://iopscience.iop.org/0953-8984/6/20/010)

J. Phys.: Condens. Matter 6 (1994) 3707–3718. Printed in the UK

Quantum oscillations and Fermi surfaces of Sn- and Pb-doped Bi

K Kilic and H Celik

Department of Physics, Hacettepe University, Beytepe, 06352 Ankara, Turkey

Received 22 December 1992, in final form 23 December 1993

Abstract. The Fermi surfaces of bismuth single-crystal samples doped with tin and lead have been investigated by means of the techniques of ultrasonic quantum oscillations (UQO) and Shubnikov–de Haas (SdH) oscillations. Experiments were carried out in the temperature range 1.2–4.2 K using longitudinal ultrasonic waves of frequencies up to 70 MHz and in magnetic fields up to 2.3 T. The excess hole densities of single-crystal samples obtained from the analysis of UQO and SdH oscillations data, residual resistivity ratio (RRR) and Hall-effect measurements are in the range of 3×10^{23} to 1.4×10^{25} m^{-3}. The Fermi-surface geometry of carriers was determined from the angular dependence of the periods of UQO and SdH oscillations. The major effect of doping of bismuth with Sn (or Pb) is to decrease the Fermi energy. On increasing the amount of doping, the pockets in the L-point conduction band became progressively smaller. Further increase of the dopant concentration leads to the disappearance of the L-electron pockets and the appearance of L holes. The experimental results have shown that the Fermi surfaces of acceptor-doped bismuth crystals are similar to those of pure bismuth and that the L_v valence band is the mirror image of the L_c conduction band.

1. Introduction

The electronic and transport properties of bismuth are very sensitive to impurities because of its low intrinsic carrier concentration (2.7×10^{23} m^{-3} at 4.2 K). Tin and lead behave like an acceptor in Bi and affect its transport properties. In tin- or lead-doped Bi with concentrations up to 0.1 at.%, the quantum oscillatory effects have been studied [1–9] and the results have been interpreted within the framework of the rigid-band model. However, the geometry of the Fermi surface of doped Bi could not be determined since detailed measurements were not available. There are only a few ultrasonic quantum oscillations (UQO) studies in Sn-doped Bi [7–9]. Giura *et al* [8, 9] observed magnetoacoustic oscillations only in a single crystal of Bi doped with Sn concentration of 4.5×10^{25} m^{-3} and proposed that these oscillations arose from a new hole band existing in the forbidden energy band gap, in addition to the T-point hole band. They also discussed the shape and symmetry of these new hole pockets.

In the present work, the band structure of Sn- and Pb-doped Bi single crystals with concentrations up to 0.1 at.% have been investigated by means of UQO and Shubnikov–de Haas (SdH) oscillations technique. Since the magnetoresistance of these samples saturates at progressively lower magnetic fields with increasing impurity concentration, it is difficult to observe the SdH oscillations in a magnetic field up to 2.3 T. Therefore, the SdH oscillations technique could not be solely employed to investigate these materials. The experimental data are discussed on the basis of the rigid-band model, which assumes that the electronic energy band structure remains quantitatively unchanged by doping at acceptor concentrations below 0.1 at.%. The Fermi-surface parameters have been determined from the angular dependence

0953-8984/94/203707+12$19.50

of measured periods of the UQO and SdH oscillations in the framework of the Lax ellipsoidal non-parabolic (ENP) model [10] for the L-point electrons and the L-point holes.

2. Theory

2.1. The Fermi surface and band structure of Bi

The electron Fermi surface of Bi consists of three identical ellipsoids at the L points of the Brillouin zone denoted by a (principal ellipsoid), b and c. The principal axis of each of these ellipsoids coincides with the binary axis of the crystal; the other two axes are tilted from the trigonal plane by an angle of about 6°. The tilt angle of the electron ellipsoids can be expressed by

$$\phi = \tfrac{1}{2}\tan^{-1}[2m_{23}/(m_{22} - m_{33})] \tag{1}$$

where m_{ij} are the components of the effective-mass tensor.

The hole Fermi surface consists of a single ellipsoid of revolution about the trigonal axis centred at the T points of the reduced Brillouin zone. The projection of the hole and electron ellipsoids onto the trigonal plane is shown in figure 1. The energy band structure of Bi at the L and T points of the Brillouin zone is given in figure 2.

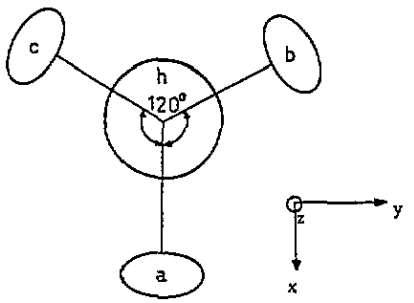

Figure 1. The projections of electron ellipsoids of Bi onto the trigonal plane.

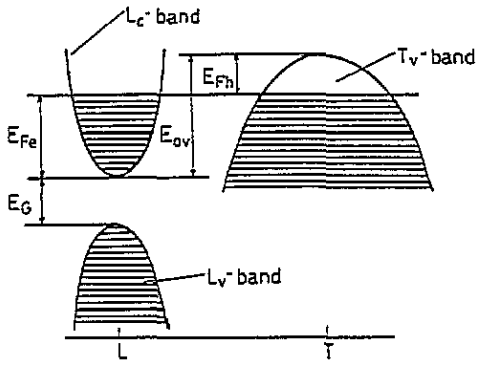

Figure 2. Schematic band structure of Bi.

Several models have been developed to explain the energy band structure of Bi [10–14]. It is possible that the ellipsoidal non-parabolic (ENP) model also applies successfully to dilute acceptor-doped Bi.

2.2. The effects of acceptors on the energy band structure of Bi

The major effect of the doping of Bi with Sn or Pb is the lowering of the Fermi level. The carrier concentrations in the L_c, L_v and T_v bands per pocket will be denoted by n_e, p_l and P_h, respectively. For the electron band in Bi, in the case of $E_{Fe} \gg kT$, the expression for the carrier density per ellipsoid is [15]

$$n_e = (8\pi 2^{3/2}/3h^3)(\det m^*)^{1/2}\Gamma^{3/2}(E) \tag{2}$$

where $\Gamma(E) = E_{Fe}(1 + E_{Fe}/E_G)$, $\det m^* = m_1 m_2 m_3 - m_1 m_4^2$ and

$$m_1 = m_{xx}/m_0 \qquad m_2 = m_{yy}/m_0 \qquad m_3 = m_{zz}/m_0 \qquad m_4 = m_{yz}/m_0.$$

The excess hole density (Δ) created by increasing the amount of acceptor added can be written as

$$\Delta = P - N = P_h + P_l - N \tag{3}$$

where $N = 3n_e$ and $P_l = 3p_l$.

The effects of increasing the acceptor density may be summarized for three different cases [16, 17]:

(i) In acceptor-doped Bi, while the number of electrons in the L_c band decreases, the number of holes in the T_v band increases and the Fermi level lowers until an acceptor concentration of 1.7×10^{24} m^{-3} is reached. In this region $P_h > N$ and $\Delta = P_h - N$.

(ii) With further addition of Sn (or Pb), the electrons in the L_c band are depleted totally. However, the T-point hole concentration continues to increase until a concentration of 2.7×10^{24} m^{-3} is reached. The Fermi level is in the energy band gap between the L_c and L_v bands. In this region, only the T-point holes contribute to the transport properties and $\Delta = P_h$.

(iii) When an acceptor concentration of 2.7×10^{24} m^{-3} is reached, the Fermi level falls below the L_v band maximum and holes begin to appear in the L_v band. In this case the created excess holes are distributed proportionally with the density of states to the L_v and T_v valence bands; the only carriers are holes and $\Delta = P_h + P_l$. When Sn or Pb concentration of 5.0×10^{24} m^{-3} is reached, the density of holes in the L_v band of the doped material becomes equal to that of electrons in the L_c band in pure Bi. This excess hole concentration corresponds to Bi doped with Sn roughly 0.018 at.%. If it is assumed that the L-point hole band is the mirror image of L_c-electron band, the relationships valid for the L-point electrons may also be used for the L-point holes. However, while E_F for the L-point electrons is measured upwards from the bottom of the L_c band, E_F for the L-point holes is to be measured downwards from the top of the L_v band.

2.3. The periods of quantum oscillations

When ultrasonic waves are propagated through metals at low temperature, the coefficient of ultrasonic wave attenuation shows oscillation with magnetic field, known as ultrasonic quantum oscillations (UQO). The part oscillating with magnetic field of magnetoresistance at low temperature is known as Shubnikov–de Haas (SdH) oscillations. The period of these oscillations is simply related to the extremal cross-sectional area of the Fermi surface normal to the magnetic field. The effect is periodic in reciprocal magnetic field ($1/H$). The period of the oscillations for an ellipsoidal Fermi surface is given by

$$\Delta(1/H) = e\hbar/m_0(C_1 \cos^2\theta + C_2 \sin^2\theta + C_3 \cos\theta \sin\theta)^{1/2}. \tag{4}$$

The data have usually been collected in two experimental configurations: with magnetic field applied in the yz plane (case I) and the xy plane (case II).

In this equation (4) the coefficients C_i for the ellipsoid a (case I) are

$$C_1 = m_3/D \qquad C_2 = m_2/D \qquad C_3 = 2m_4/D \tag{5}$$

and for the ellipsoids b and c are

$$C_1 = m_3/D \qquad C_2 = (3m_1 + m_2)/D \qquad C_3 = -m_4/D. \tag{6}$$

Here $D = (m_1 m_2 m_3 - m_1 m_4^2)\Gamma(E)$ and m_{ij} are the components of the effective-mass tensor. The magnetic field direction (θ) is measured from the z axis.

In case II, the coefficients C_i for the ellipsoid a are

$$C_1 = m_2/D \qquad C_2 = m_1/D \qquad C_3 = 0 \tag{7}$$

and for the ellipsoids b and c are

$$C_1 = (3m_1 + m_2)/4D \qquad C_2 = (m_1 + 3m_2)/4D \qquad C_3 = \pm\sqrt{3}(m_1 - m_2)/2D \tag{8}$$

where the minus sign corresponds to the pocket b, the plus sign to the pocket c and the magnetic field direction (θ) is measured from the x axis.

For $\boldsymbol{H} \| yz$ plane (case I), the angular dependence of the periods of T_v holes is given by

$$\Delta(1/H) = e\hbar/E_{Fh}m_0c(C_1\cos^2\theta + C_2\sin^2\theta)^{1/2} \tag{9}$$

where θ is measured from the z axis. The coefficients C_i are

$$C_1 = 1/M_1M_2 \qquad C_2 = 1/M_1M_3 \tag{10}$$

where M_{ij} are the components of the effective-mass tensor of T_v holes.

3. Experimental procedures

The single crystals of Bi, Bi–Sn and Bi–Pb were grown by the zone-levelling technique using 5N purity Bi, Sn and Pb. The rate of motion of the zone was chosen to avoid a cellular substructure as a result of constitutional supercooling. The orientations of the single crystals were determined by the Laue x-ray technique and by studying the pattern of etch pits and slip lines on the cleavage plane, which guided the identification of the bisectrix and binary axes [18–20]. The error in the orientation of the crystals by this method is within $\pm 0.5°$. The samples were prepared from oriented crystals by using a spark cutter and planer (Servomet SDM). The samples were annealed in the temperature range 200–250 °C under vacuum for one week.

The carrier density and the corresponding atomic percentages of some of the samples under study were determined by measuring the high-field Hall coefficients at 4.2 K. As has been noted by some workers [21, 22], we too observed that the residual resistance ratio (RRR) exhibits a behaviour that depends on Δ. This relation between RRR and Δ can be used to determine the excess hole density of the sample at 4.2 K. The excess hole density of the samples was obtained from the analysis of UQO and SdH oscillations as shown in table 1. These values of Δ are in reasonable agreement with those obtained from the Hall coefficient and RRR measurements.

X-cut quartz transducers with fundamental frequency of 10 MHz were used to propagate and detect the longitudinal ultrasonic waves of frequency 10–70 MHz. The sound wavevector (q) was chosen along the z axis and y axis. Changes in the ultrasonic attenuation were detected by a Matec ultrasonic system (model 9000 and 2470). Magnetic fields up to 2.3 T were obtained by an electromagnet (Varian model 3800). The ultrasonic attenuation and magnetoresistance measurements were made in the temperature range 1.2–4.2 K.

Table 1. The coefficients C_i obtained from the angular dependences of the oscillation periods.

Experimental conditions	Sample	Δ[a] (10^{23} m^{-3})	Pocket a (and A)			Pockets b, c (and B, C)		
			C_1	C_2	C_3	C_1	C_2	C_3
$q\|\|z$ and $H\|\|yz$	Bi		1.143	60.0	12.68	1.56	14.25	−5.95
	S2	3.2(e)	0.943	88.0	13.05	1.90	23.49	−11.02
	S3	4.5(e)	1.992	110.0	24.42	1.33	27.61	−15.03
	R4	6.5(e)	2.382	127.9	25.42	2.87	37.23	−3.78
	R1	~15(e)[b]	−5.37	204.6	52.82	−0.33	50.51	−30.77
	P1	~40(h)[b]	−3.357	104.7	35.56			
	P2	52.1(h)	1.297	49.3	10.43	1.29	12.24	−5.90
	P4	79.5(h)	0.275	21.3	3.78	0.75	5.13	−1.14
	P7b	141(h)	0.161	3.6	0.81			
$q\|\|z$, y and $H\|\|xy$	P4	79.5	0.167	18.87	0	14.19	4.84	±16.2[c]

[a] Excess hole density (e) in the L_c band (a, b and c electron pockets), and (h) in the L_v band (A, B and C hole pockets).

[b] These Δ values were determined from Hall-coefficient measurements.

[c] The minus sign corresponds to pocket B and the plus sign corresponds to pocket C.

4. Results and discussion

The effects of increasing Sn concentration on UQO are illustrated in figure 3. The curves in this figure were obtained under the same experimental conditions. The periods of oscillations first increase and then decrease with increasing Sn concentration.

The UQO observed in these samples usually give information about the pockets at the L point of the Brillouin zone. However, the SdH oscillations observed in the resistance samples cut from the neighbourhood of ultrasonic samples belong to the T_v hole pocket.

The periods have been found from Fourier analysis. In most cases the nominal error in the measured periods is expected to lie within 1–10 at.%.

The excess hole density of R4 was determined as $\Delta = 6\times10^{23}$ m^{-3} from Hall-coefficient measurements, so its Fermi level is in the L_c conduction band. Typical experimental results for UQO observed in this sample and SdH oscillations observed in sample R4e1, which was prepared from the neighbourhood of R4, are given in figure 4. The angular dependences of the UQO and SdH oscillation periods for the electron pockets (a, b, c) and hole pocket of this sample in the yz plane are shown in figure 5. The periods corresponding to the electron pockets are larger than those pure Bi.

The excess hole density of sample R1 was determined as $\Delta = 1.5 \times 10^{24}$ m^{-3}. The Fermi level of this sample falls within but near the bottom of the L_c-electron band. An example of the UQO observed in this sample is given in figure 3.

An example for the UQO observed in sample P2 is shown in figure 3. The Fermi level of this sample falls within the L_v band. The angular dependence of the periods is shown in figure 6. The theoretical curve passing through the experimental points is defined by equation (4), which is written for the electron pockets a, b and c at the L point. The agreement between the theoretical curves and the experimental data shows that the symmetry of the L-point hole bands is the same as that of L-electron bands. Therefore the hole pockets at the L point are labelled as A, B and C. In this case, the pocket A corresponds to the principal hole pocket in the L point. This shows that we could use the ENP model for the L_v valence band as well.

In sample P4, UQO were also observed in the following conditions: (i) $q\|y$ and $H\|xy$ plane and (ii) $q\|z$ and $H\|xy$ plane. The angular dependences of the periods of

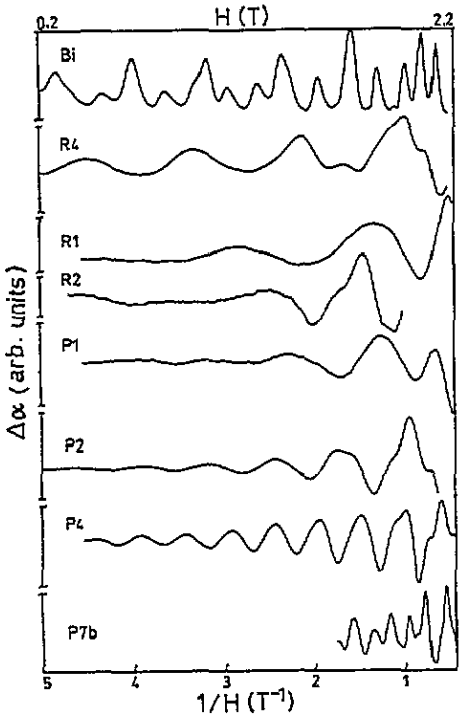

Figure 3. The effects of increasing Sn concentration on UQO under the same experimental conditions: $\theta = 60°$, $q \| z$, $H \| yz$ plane, $T = 4.2$ K. The scale is different for each of the curves.

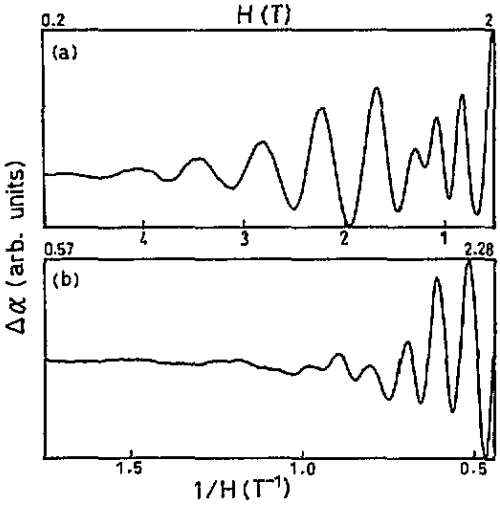

Figure 4. (*a*) The change in the attenuation coefficient ($\Delta\alpha$) as a function of $1/H$: sample R4 (Bi–Sn, $\Delta = 6.5 \times 10^{23}$ m^{-3}); $q \| z$, $H \| yz$ plane, $\theta = 145°$, $f = 50$ MHz, $T = 4.2$ K. (*b*) Recorder trace showing SdH oscillations against $1/H$ for $I \| x$, $H \| yz$ plane: sample R4e1; $\theta = 10°$, $T = 4.2$ K.

UQO observed in these conditions are shown in figure 7. It can be seen that the L_v-hole pockets have the same symmetry as that of the a and b, c electron pockets of pure Bi in the xy plane.

The excess hole densities of Pb-doped samples S2 and S3 were calculated from Hall-coefficient measurements as $\Delta = 3 \times 10^{23}$ m^{-3} and $\Delta = 4.5 \times 10^{23}$ m^{-3} respectively. According to these values, the Fermi levels of these samples are in the L_c band. A typical example of UQO that show contributions from different pockets for samples S2 and S3 is given in figure 8.

Now, we can discuss the results of this experimental work in detail. The periods of UQO observed in Bi–Sn samples, for $H \| yz$ plane, fall on two different curves (figures 5 and 6). The shape and the symmetry of these curves show that these carrier pockets have the same properties as the image of the electron pockets of Bi in this plane. Therefore we propose that there are ellipsoidal hole pockets located at the L point and which are tilted from the trigonal plane.

The angular dependence of the periods for the principal ellipsoids of the Sn-doped samples along with that of Bi in the yz plane are shown in figure 9. The samples whose Fermi level falls in the L_c conduction band is compared in figure 9(*a*). These samples have periods larger than that of Bi. The oscillation period increases with increasing Sn concentration. In figure 9(*b*), the samples whose Fermi level falls in the L_v valence band

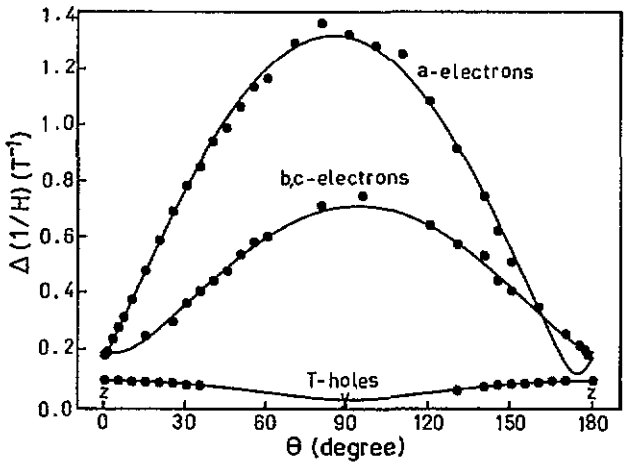

Figure 5. Angular dependence of oscillation periods for sample R4 (Bi–Sn) in the yz plane. The full circles correspond to the experimental data. The full curves are the best fits of equation (4). The pockets are specified in each curve. The period values of T hole pocket are obtained from SdH oscillations.

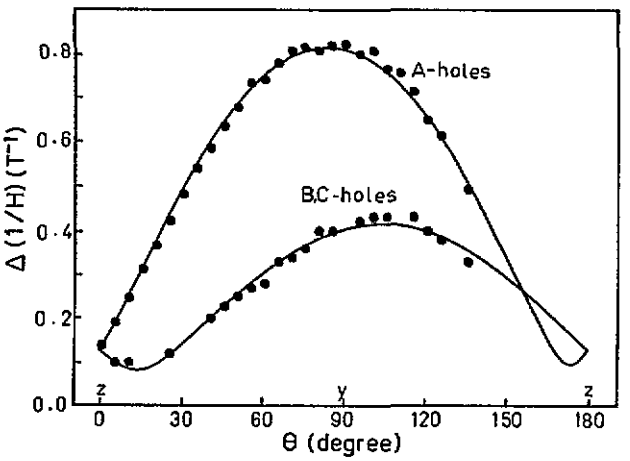

Figure 6. Angular dependence of oscillation periods for sample P2 (Bi–Sn) in the case $q \| z$ and $H \| yz$ plane. The full curves are the best fits of equation (4). The L-hole pockets are specified in each curve.

is compared with pure Bi. The periods of doped samples are smaller than that of Bi; an exception is sample P1. Until the Fermi level reaches the mirror symmetry of the Fermi level of Bi in the L_v band (the Fermi level is taken downwards from the top of the L_v band), the L-point hole pockets are smaller than L-point electron pockets of Bi. If the Fermi levels shift below from the mirror symmetry of Bi in L_v-hole band, the cross sections of L-point hole pockets increase and, therefore, the period values become smaller.

The full curves in figures 5, 6, 7 and 9 are the best fits of equation (4) to the experimental data points. The coefficients C_i defining the curves are given in table 1 for L_c electrons and L_v holes. The measured periods and those calculated by using the parameters C_i are within

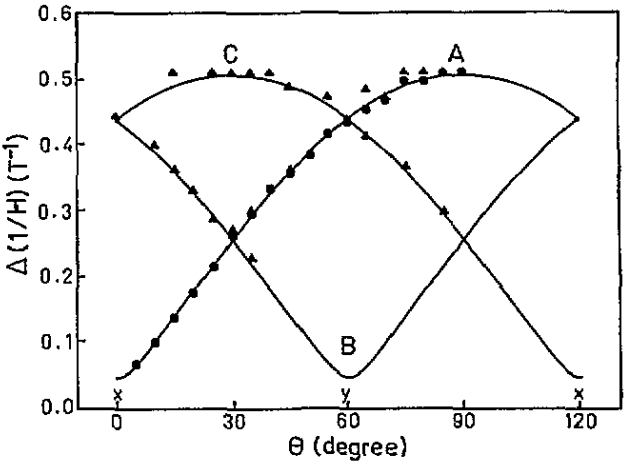

Figure 7. *Angular dependence of oscillation periods for sample* P4 (Bi–Sn) *in the case* $H \| xy$ plane. The full triangles are for $q \| z$, which was obtained by Fourier analysis, and the full circles are for $q \| y$, which was obtained with linear regression. The pockets are specified in each curve.

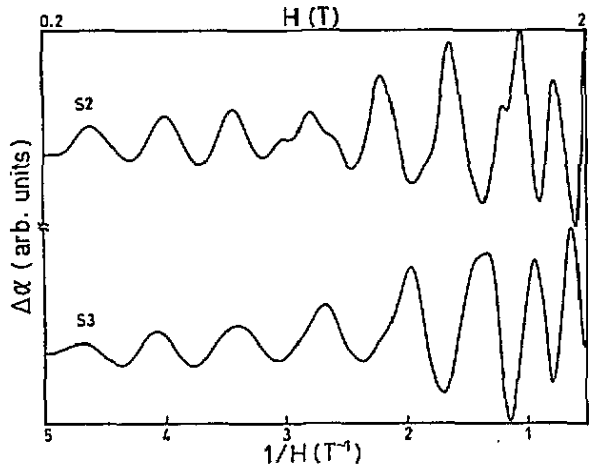

Figure 8. Comparison of the UQO obtained in samples S2 (Bi–Pb, $\Delta = 3 \times 10^{23}$ m^{-3}) and S3 (Bi–Pb, $\Delta = 4.5 \times 10^{23}$ m^{-3}) under the same experimental conditions: $\theta = 140°$, $q \| z$, $H \| yz$ plane, $T = 4.2$ K. The scale is different for the two curves.

±3% in most of the orientations. The effective masses (in units of m_0) for the principal ellipsoid in the crystal axis system and the value of $\Gamma(E)$ have been obtained from the parameters C_i using equation (5) by successive approximation with an accuracy of 0.1%. The Fermi energy is calculated assuming that the energy gap does not vary with doping, i.e. $E_G = 13.6$ meV. The results are given in table 2.

The SdH oscillations observed in sample R4 originate mainly from the T holes. The period of these oscillations is compared with T holes of Bi in figure 10. The components of the effective-mass tensor of T holes are obtained as $M_1 = M_2 = 0.0524$ and $M_3 = 0.51$.

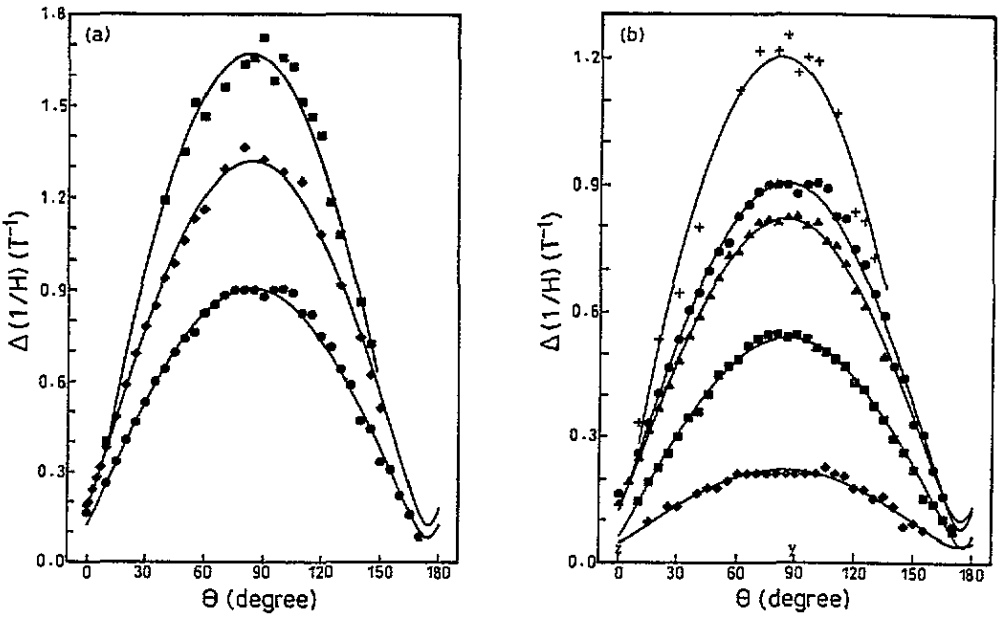

Figure 9. Concentration and angular dependence of the oscillation periods for the principal ellipsoid of Sn-doped Bi samples in the *yz* plane of (*a*) samples whose Fermi level falls within the L_c band (squares correspond to sample R1, diamonds to sample R4, circles to pure Bi) and (*b*) samples whose Fermi level falls within the L_v band (crosses correspond to sample P1, circles to pure Bi, triangles to sample P2, squares to sample P4, diamonds to sample P7b).

The Fermi energy of T holes (E_{Fh}) is obtained as 22.8 meV from SdH oscillations data. The Fermi energy of electrons (E_{Fe}) in R4 is obtained as 15.8 meV from UQO data (table 2). The value E_{Fh} calculated from this value is 22.6 meV. These results obtained from different techniques are in reasonable agreement.

The carrier densities in the L-point electron pockets and the L-point hole pockets (N_e and P_h) are calculated by using the values of m_i and $\Gamma(E)$ in equation (2). The results are summarized in table 2. The excess hole densities (Δ) in the samples are calculated considering the discussion in section 2.2. The values of N, P_l and Δ are also given in table 2. The Fermi energies in the last column of table 2 are measured from the bottom of the L_c band. The dependence of the Fermi energy on the excess hole density is calculated using the effective-mass components of Bi (table 2). The results are represented by the full curve in figure 11. The band structure of Bi is also shown schematically on the same figure. The values of Δ and E_F (table 2) are also shown in figure 11. The data obtained for the present samples are in reasonable agreement with the rigid-band model.

The tilt angle (ϕ) of the ellipsoids calculated from equation (1) using the effective-mass tensor are presented in table 2. The variations in the tilt angle are within the experimental error of crystal orientation; the tilt angle in the acceptor-doped samples are close to that in pure Bi.

5. Conclusions

The T-hole pocket has a rather larger volume than those at the L point. Therefore, the effect of the excess hole density created by acceptor doping on the T_v band is smaller than the

Table 2. The band parameters calculated from the coefficients C_i of Bi and of Sn- and Pb-doped Bi samples.

Sample	Alloy	m_1	m_2	m_3	m_4	$\Gamma(E)$ (meV)	E_F [a] (meV)	ϕ (deg)	N (or P) (10^{23} m^{-3})	Δ (10^{23} m^{-3})	E_F [b] (meV)
Bi[c]		0.00102	0.224	0.00526	0.0236	81.5	27.2(e)	6.1	2.53		27.2
S2	Bi–Pb	0.00195	0.412	0.00441	0.0305	52.0	20.7(e)	4.3	2.14	3.2	20.7
R4	Bi–Sn	0.00258	0.295	0.0055	0.0293	34.2	15.8(e)	5.7	1.21	6.5	15.8
P2	Bi–Sn	0.00111	0.205	0.00529	0.0217	78.0	26.5(h)	6.1	2.46	52.1	−40.1
P4	Bi–Sn	0.00045	0.114	0.00290	0.0112	242.0	51(h)	5.7	4.83	79.5	−64.6
P7b	Bi–Sn	0.00033	0.044	0.00198	0.0050	768.0	95.6(h)	6.6	13.2	141.0	−109.2

[a] Measured (e) upwards from the bottom of the L_c-electron band, and (h) downward from the top of L_v-hole band.
[b] Measured from the bottom of the L_c-electron band.
[c] Reference [20].

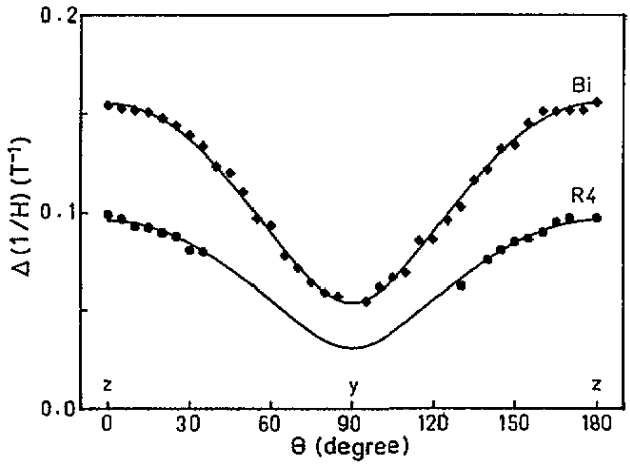

Figure 10. Comparison of the angular dependence of the SdH oscillation periods belonging to T holes of sample R4 (Bi–Sn) and pure Bi in the *yz* plane. The full curves are the best fits of equation (9).

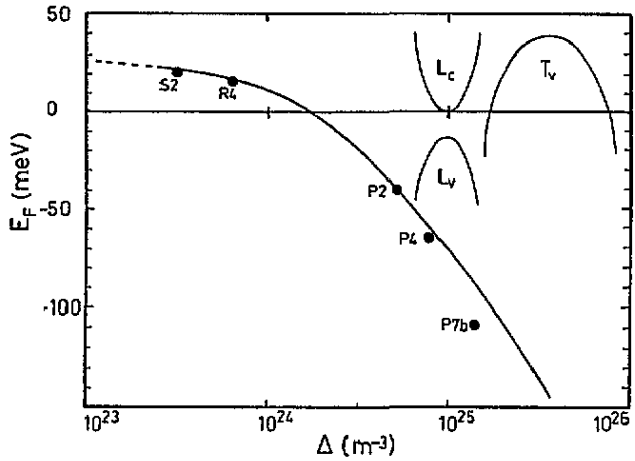

Figure 11. The variation of Fermi energy with excess hole density (Δ). The full curve was obtained using the data for Bi. The band structure of Bi is shown schematically on the same figure. The Fermi energy is measured from the bottom of the L_c band.

effect created on the L bands. On the other hand, when the dependence of magnetoresistance on magnetic field was investigated, it was seen that magnetoresistance saturates at 4.2 K, i.e. becomes independent of magnetic field, and the field value at which the magnetoresistance saturates decreases with increasing Δ. In the region where the magnetoresistance saturates, SdH oscillations disappear. Therefore the SdH studies were confined in a region about the z axis. Consequently, it was difficult to enquire about the L-point bands from the SdH oscillations. The SdH oscillations originate mainly from the T-hole pocket. However, the UQO provide information mainly about the L bands; thus the geometry of the L-point bands has been investigated in detail. The experimental results show that the ENP model that is

valid for the L_c-electron band of Bi can also be applied to the L_v-hole band. In particular, the results obtained on sample P4 support the suggestion that the L bands are the mirror image of each other. Consequently, if the Fermi energy is measured downwards from the top of the L_v band, the relations written for electrons can also be used for the L-point holes. Giura *et al* [8,9] observed magnetoacoustic oscillations in a single crystal of Bi doped with Sn at a concentration of 4.5×10^{24} m^{-3}. They proposed that this concentration corresponds to the band gap in the L point and that the oscillations observed originate from a new hole band created in the energy gap. However, the results of present UQO measurements made on three samples with different Sn concentrations, for which the Fermi level is in the L_v band, did not show evidence for the presence of a hole pocket in the band gap. The present results show that the Fermi surfaces of acceptor-doped bismuth crystals are similar to those of pure Bi and, depending on the dopant concentration, these pockets are altered isotropically.

Acknowledgments

We are grateful to Hacettepe University Research Fund (project number 88.03.010.003) for financial support. We would like to thank Dr M Onder and Dr M Cankurtaran for careful reading of our manuscript.

References

[1] Brand N B and Razumeenko M V 1961 *Sov. Phys.–JETP* **12** 198
[2] Bhargava R N 1967 *Phys. Rev.* **156** 785
[3] Woo On-Ting and Balcombe R J 1968 *Can. J. Phys.* **46** 2413
[4] Bate R T and Einspruch N G 1967 *Phys. Rev.* **153** 796
[5] Bate R T, Einspruch N G and May P J 1969 *Phys. Rev.* **186** 599
[6] Brand N B, Muller R and Ponomarev Ya G 1976 *Sov. Phys.–JETP* **44** 1196
[7] Giura M and Marcon R 1970 *Phys. Rev.* B **1** 1528
[8] Giura M, Marcon R, Presutti E and Scacciatelli E 1972 *J. Phys. C: Solid State Phys.* **5** 2405
[9] Giura M, Marcon R, Presutti E and Scacciatelli E 1972 *J. Phys. C: Solid State Phys.* **5** 3073
[10] Lax B, Mavroides J G, Zeiger H J and Keyes R J 1960 *Phys. Rev. Lett.* **5** 241
[11] Lax B and Mavroides J G 1960 *Solid State Physics* vol 11, ed F Seitz and D Turnbull (New York: Academic) pp 261–400
[12] Cohen M H 1961 *Phys. Rev.* **121** 387
[13] McClure J W and Choi K H 1977 *Solid State Commun.* **21** 1015
[14] Cankurtaran M, Onder M, Celik H and Alper T 1987 *J. Phys. C: Solid State Phys.* **20** 3875
[15] Issi J P 1979 *Aust. J. Phys.* **32** 585
[16] Heremans J 1978 *PhD Thesis* Université Catholique de Louvain, Belgium
[17] Misu A, Chieu T C, Dresselhause M S and Heremans J 1982 *Phys. Rev.* B **25** 6155
[18] Akgoz Y C and Saunders G A 1971 *J. Mater. Sci.* **6** 395
[19] Kilic K and Celik H 1993 *Doga-Tr. J. Phys.* **17** 513
[20] Cankurtaran M, Celik H and Alper T 1985 *J. Phys. F: Met. Phys.* **15** 391
[21] Boxus J, Heremans J, Micenaud J P and Issi J P 1979 *J. Phys. F: Met. Phys.* **9** 2387
[22] Uher C 1979 *J. Phys. F: Met. Phys.* **9** 2399